Algorithm and System Development for Robotic Micro-Volume Herbicide Spray Towards Precision Weed Management

Chengsong Hu¹⁰, Shuangyu Xie¹⁰, Dezhen Song¹⁰, Senior Member, IEEE, J. Alex Thomasson, Robert G. Hardin IV, and Muthukumar Bagavathiannan¹⁰

Abstract—Weed competition is one of the most limiting factors affecting crop yield and profitability. Robotic weeding systems have demonstrated their potential to save herbicide usage and thereby minimize costs and adverse impacts on the environment. We introduce the software and hardware design of an automatic system for micro-volume herbicide spray using a mobile robot for early-stage weed control. The system is equipped with a stereo camera, one inertial measurement unit, and multiple linearly actuating spray nozzles. To enable the system, we propose a new scene representation from the perspective of spray operation. We represent the space occupied by weeds as candidate line segments for spray and then construct a directed acyclic graph (DAG) that embraces the feasible nozzle paths among weeds. Based on the new scene representation, we formulate an optimal K-nozzle assignment/motion planning problem and develop a binary linear programming-based algorithm to assign nozzles to the candidate line segments for optimal coverage. We built the system and conducted both simulation and field experiments. Evaluation on rough soil surfaces with artificial targets has shown that the lateral errors of herbicide spray are at sub-centimeter levels. Simulation results demonstrate that the proposed assignment algorithm can provide good coverage within the intra-row regions.

Index Terms—Agriculture automation, motion and path planning, precision agriculture, spray nozzle assignment, weeding robot.

Manuscript received 28 February 2022; accepted 24 June 2022. Date of publication 15 July 2022; date of current version 14 September 2022. This letter was recommended for publication by Associate Editor P.-C. Lin and Editor H. Moon upon evaluation of the reviewers' comments. This work was supported in part by the National Science Foundation - United States Department of Agriculture (NSF-USDA) National Robotics Initiative 3.0 grant under Award 2021-67021-35959. (Chengsong Hu and Shuangyu Xie are co-first authors.) (Corresponding authors: Muthukumar Bagavathiannan; Dezhen Song.)

Chengsong Hu is with the Department of Biological and Agricultural Engineering, Department of Soil and Crop Sciences, Texas A&M University, College Station, TX 77843 USA (e-mail: huchengsong@tamu.edu).

Shuangyu Xie and Dezhen Song are with the Computer Science and Engineering Department, Texas A&M University, College Station, TX 77843 USA (e-mail: sy.xie@tamu.edu; dzsong@cs.tamu.edu).

Robert G. Hardin IV is with the Department of Biological and Agricultural Engineering, Texas A&M University, College Station, TX 77843 USA (e-mail: rghardin@tamu.edu).

Muthukumar Bagavathiannan is with the Department of Soil and Crop Sciences, Texas A&M University, College Station, TX 77843 USA (e-mail: muthu@tamu.edu).

J. Alex Thomasson is with the Department of Agricultural and Biological Engineering, Mississippi State University, Starkville, MS 39762 USA (e-mail: athomasson@abe.msstate.edu).

This letter has supplementary downloadable material available at https://doi.org/10.1109/LRA.2022.3191240, provided by the authors.

Digital Object Identifier 10.1109/LRA.2022.3191240

I. INTRODUCTION

EED competition is one of the most limiting factors affecting crop yield and profitability. Weeds cause the highest crop yield loss (34%) among all agricultural pests when not managed well [1]. Current challenges in weed management due to high labor demand, over-application of herbicides, and limited availability of alternative control methods can be potentially alleviated by the introduction of autonomous weeding robots [2]. Herbicide-based weed control remains the most efficacious and economical approach, though with significant environmental consequences and high risks for the evolution of herbicide-resistant weeds [3], [4]. Traditionally, herbicides are broadcasted across the entire production field, leading to more herbicide use than necessary and frequent off-target movement onto sensitive crops.

Designing an accurate, real-time, and economical autonomous weeding system relies on three key components: a perception system detecting and representing weeds, a decision-making unit processing the perception output and making actuation decisions, and a group of actuators performing weed control actions accordingly [3]. However, common weed/crop descriptions used in plant detection cannot be directly used for actuation planning. The raw output of detection generally does not balance weed localization and key information abstraction (e.g., geometrical shape) well [5]. Currently, a weed/crop scene representation that incorporates both plant geometry and actuator feasibility constraint is absent. A lack of such scene representation prevents the design of a good planning algorithm for efficient and precise weed control

The major contribution of our work is a real-time robotic herbicide spray system with two novel algorithms and a complete hardware platform. Firstly, we construct a tri-layer scene representation by abstracting DAGs from plant occupancy maps through intermediate line segments. Based on the new scene representation, we formulate an optimal K-nozzle assignment/motion planning problem and develop a binary linear programming-based algorithm to assign nozzles to the line segments for windowed optimal coverage with the deadline introduced by the robot motion. To achieve full herbicide spray functionality, we implement the proposed algorithms on a low-cost hardware platform equipped with linearly actuated nozzles.

U.S. Government work not protected by U.S. copyright.

We have built the system and evaluated its performance. Simulation and field experiments show that our system is able to work in real-time, maximize spray coverage of weeds growing within 10 cm of the crop plants, and achieve spray accuracy at sub-centimeter levels. Compared to the existing system of [6], our herbicide spray system uses a simpler hardware design regarding the sensor suite, while allowing the system to travel twice as fast owing to our efficient scene representation and planning algorithms.

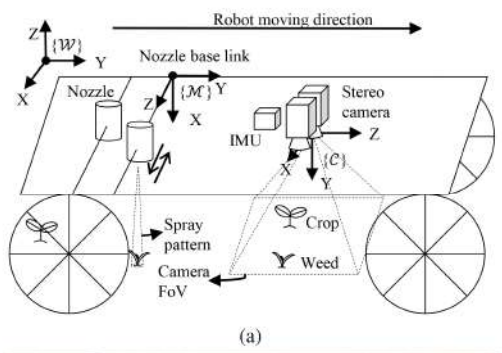
II. RELATED WORK

Agricultural robots: Extensive research has been performed on various aspects of agricultural robot development, such as scene perception [5], [7], [8], robot navigation [9], motion planning [10], and deployability of aerial/ground platforms [11]–[13]. Existing work has solved a great number of important problems, providing foundations for the design of more capable agricultural robots. However, since most of the robots are designed for large-field operations with coarse perception granularity, it is challenging to directly adopt them for applications where centimeter-level accuracy is required.

Robotic weed control: Developing systems for weed control is one of the major research fields in agricultural robotics. Much effort is focused on the development of crop/weed detection methods and control mechanisms. Actuation methods that have been extensively evaluated include mechanical cultivation, thermalbased actuation, abrasion, mowing, and herbicide spray [2]. Attempts have been made by several research groups to develop robotic spray systems [14]-[16] utilizing nozzle arrays and 2D spray maps generated from machine vision systems. However, using an array of nozzles is not cost-effective, considering the number of nozzles needed to provide enough resolution within the narrow intra-row region. Recently, Wu et al. [6] deployed a complicated non-overlapping multi-camera system to perform weed detection and tracking for herbicide spray and stamping. Weeds are represented as shapeless points, and a single pulse or stamp is applied to a weed when it reaches the actuators.

Scene representation: Building a precise and efficient scene representation for real-time systems has been a major challenge. Recent developments in computer vision have made real-time detection algorithms such as YOLOv5 [17] readily available. The output of state-of-the-art plant detection algorithms is often in the form of a single point [6], bounding box [18], or pixel/point cloud [11]. Pixel/point clouds provide rich geometric information but require heavy computation, while single points overly condense the information, giving up important geometric properties for actuation planning. For this reason, many existing agricultural robots convert the raw perception results into primary shapes for better scene understanding [11], [18]. For multiactuator planning, the constraints of actuators such as kinematic limits also need to be considered. To achieve efficient planning for real-time systems, a representation that preserves precise weed/crop description and incorporates actuator constraints is needed.

Constrained Planning & Assignment Problem: There is much progress in the development of planning algorithms for painting



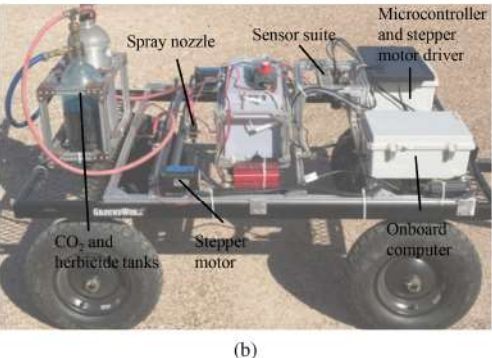


Fig. 1. (a) System overview and 3D coordinate systems. (b) Hardware platform.

nozzles to achieve a complete and uniform coverage [19], [20]. In those tasks, trajectories are generated to achieve the exactness and smoothness of painting. Although painting and spraying weeds share many similarities, our application requires a good assignment of multiple linearly-actuated nozzles to cover weeds with different priority levels. Our work is closely related to job scheduling and covering problems with temporal and spatial constraints [21], [22]. Similar problems also include sorting items on a moving conveyor belt using robotic arms [23] and capacitated vehicle routing with geometric constraints [24]. Despite the similarity, those problems treat every target equally, which differs from our application. Inspired by those planning algorithms and facing new field challenges, we develop a new assignment algorithm for multi-nozzle planning for herbicide spray applications.

III. SYSTEM DESIGN

The proposed spray system is mounted on a mobile agricultural robot and performs perception-guided micro-volume herbicide application using nozzles that can be independently and linearly actuated to perform lateral motion (Fig. 1(a)). To enable the hardware system, we design the software system (Fig. 2) that efficiently represents the perceived weeds and generates trajectories for the nozzles to follow. In this section, we introduce the hardware and software design of the system (see the video attachment for more details).

A. Hardware Design

The hardware system consists of three major components: i) a sensing suite composed of a stereo camera pair and an IMU,

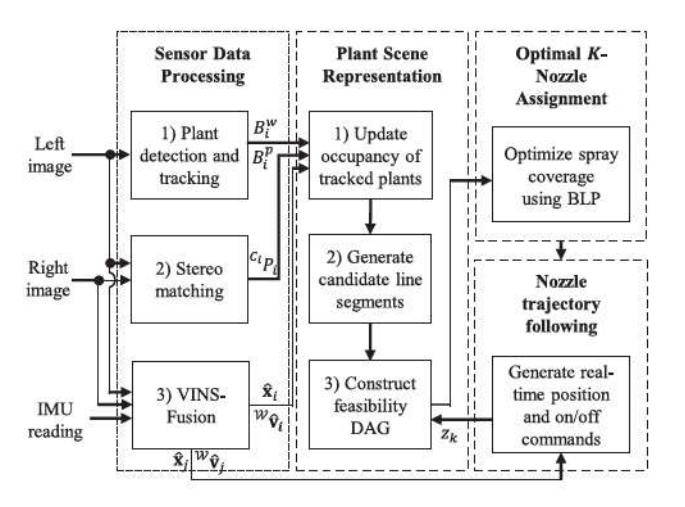


Fig. 2. Software diagram of the robotic system.

ii) an onboard computer, and iii) a herbicide spray subsystem. The layout of each component is illustrated in Fig. 1(a) and (b). Considering the challenging scenarios where small weeds need to be precisely sprayed on uneven soil surfaces, we use stereo vision to obtain reliable 3D positioning of weeds. The two cameras (BlackflyTMS BFS-U3-19S4) form a stereo pair with a baseline distance of 3.45 cm and face the ground perpendicularly at the height of 0.6 m with a field of view (FoV) of 0.6×0.45 m² on flat ground. The IMU (Analog DevicesTMADIS16460) has 6 degrees of freedom (DoFs) and provides measurements of acceleration and angular velocity at 256 Hz. The onboard computer (NvidiaTM Jetson AGX Xavier) synchronizes the camera shutters and the IMU, and performs onboard data processing. The herbicide spray subsystem receives information from the onboard computer and performs micro-volume herbicide application. It consists of a microcontroller, a carbon dioxide (CO₂) tank, a herbicide tank, and several spray nozzles. Without loss of generality, we have mounted two nozzles using two independent parallel prismatic joints that move laterally with respect to the robot forwardmotion direction. Solenoid valves are employed to turn on/off the nozzles. The height of the nozzles is 0.4 m, which allows the herbicide droplets to sufficiently cover a seedling weed.

B. Software Design

The main components of the software are summarized in Fig. 2. The key requirement for the software is that it localizes weeds in the 3D space and generates nozzle actuation commands. Naturally, there is a time delay between the observation of weeds and the actuation of nozzles. This time delay allows the computer to process the sensor inputs and generate optimal trajectories for nozzles to follow, but meanwhile requires the robot to rapidly estimate its state change so that nozzles are triggered at the desired time and position.

The software consists of four major components, the first one being the process of sensor data. Plants in the images are detected using the YOLOv5 framework [17]. An object tracking framework SORT [25] is used to establish a frame-to-frame

association of the detected plants. A point cloud is generated from the disparity map calculated by the Semi-Global Matching algorithm [26] from each stereo image pair. All these three algorithms run at the imaging frequency. For robot state estimation, we adopt the VINS-Fusion framework, a sliding window-based state estimator [27], to generate state estimation at the IMU rate of 256 Hz.

In the component for scene representation, the tracked plant detection is combined with the point cloud to estimate the space occupancy of each plant in the world frame. The space occupied by weeds in the scene is abbreviated into candidate line segments, upon which a DAG is constructed to represent nozzle movement feasibility among weeds. It is often the case that the number of weeds exceeds the spray capacity of nozzles. In such cases, more emphasis is placed on the weeds that are close to the crops. We develop an algorithm to optimize spray coverage near crops using binary linear programming (BLP). The last component of the software ensures that the nozzles follow the assigned trajectory once the weeds have been assigned.

Besides the system development, our main algorithmic contributions are the modeling of the weed scene and the algorithm for nozzle assignment. In the following section, we will detail each of them. The real-time approach for nozzle trajectory following is also discussed briefly.

IV. NOTATION AND PROBLEM DEFINITION

The common notations in this paper are defined as follows. Note that all coordinate systems are right-handed.

- Define i as the robot decision index which is also the image timestamp index. Define j as the index of IMU reading timestamp.
- {W} and {C} denote the world and left camera coordinate frames, respectively. For simplicity, we let {C} coincide with the body frame. The Z-axis of {C} points to the front of the robot and Y-axis points downward. {C_i} denotes the camera frame at timestamp i.
- We let all nozzles share the same base link frame {M}.
 Its Z-axis is parallel to the nozzle movable direction and X-axis is parallel to the nozzle spray direction. We use {M_i} to denote the nozzle base frame at timestamp i.
- For a variable or vector a, â denotes the estimated state
 of a. ã denotes the homogeneous representation of a. à
 denotes the derivative of a w.r.t. time.
- $\mathbf{x}_i \in SE(3)$ denotes robot pose and contains the position $[x_i, y_i, z_i]^\mathsf{T}$, and the orientation of $\{\mathcal{C}_i\}$ w.r.t. $\{\mathcal{W}\}$. ${}^{\mathcal{W}}\mathbf{v}_i = [\dot{x}_i, \dot{y}_i, \dot{z}_i]^\mathsf{T}$. Similarly, $\mathbf{x}_j \in SE(3)$ and ${}^{\mathcal{W}}\mathbf{v}_j = [\dot{x}_j, \dot{y}_j, \dot{z}_j]^\mathsf{T}$. As a convention, left superscript of a notation indicates the reference frame.

Due to the high diversity of agricultural environments, we have the following assumptions:

- a.0 The robot predominantly moves in one direction.
- a.1 The robot operates in early-stage crops with a low density of seedling weeds and there is no significant overlap between plants.

After the i^{th} stereo image pair is captured by the stereo camera, we use its left camera image for recognition by applying

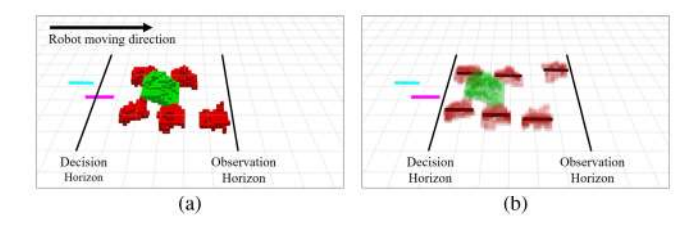


Fig. 3. (a) Discretized occupancy map of crops (green) and weeds (red) currently within the camera FoV. The cyan and purple lines represent the trajectory line segments for different nozzles to spray. (b) Unassigned line segments shown in black overlaid on top of the weed occupancy maps.

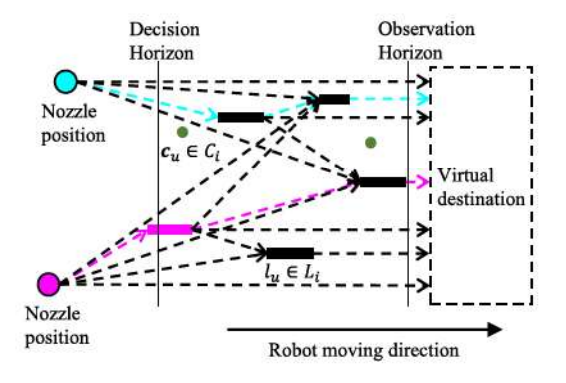


Fig. 4. Illustration of the DAG constructed for nozzle assignment. Optimal paths are in cyan and purple color. Decisions are made only for the weeds reaching the decision horizon. For better visualization, the virtual destination is illustrated as a rectangle instead of a point.

YOLOv5 and SORT. This results in two sets of classified 2D bounding boxes: crop set B_i^p and weed set B_i^w . Stereo matching produces a point cloud $^{\mathcal{C}_i}P_i$ for each stereo image pair. VINS-Fusion produces the camera-rate $\hat{\mathbf{x}}_i$ and $^{\mathcal{W}}\hat{\mathbf{v}}_i$, as well as the IMU-rate $\hat{\mathbf{x}}_j$ and $^{\mathcal{W}}\hat{\mathbf{v}}_j$.

Let l denote a line segment defined by two points in $\{W\}$ indicating the start and end positions of herbicide spray for a weed. Our problem is defined as:

Problem 1: Given sequences of B_i^p , B_i^w , C_iP_i , $\hat{\mathbf{x}}_i$, and $^W\hat{\mathbf{v}}_i$, generate a trajectory defined by a line segment sequence $S_k = (l_1, l_2, \ldots)$ for each nozzle k to maximize weed coverage near crops.

To solve this problem, we begin with the modeling of the weed scene from the spray operation perspective.

V. ALGORITHMS

A. Scene Representation for Crops and Weeds in Field

An accurate and efficient understanding of a crop/weed scene is the foundation of motion planning for weed control. We represent the scene using three layers with increasing semantics: 1) geometrical occupancy of plants cumulatively constructed from the point cloud of each image frame (Fig. 3(a)); 2) an intermediate representation consisting of candidate trajectory line segments for the nozzles to follow (Fig. 3(b)); and 3) a high-level graph that represents the feasible nozzle paths taking into consideration the nozzle kinematics and positions (Fig. 4).

The tri-layer scene representation is constructed for each stereo image pair at the imaging frequency.

- 1) Occupancy Map Generation: To handle the possible sway of plants due to wind and the uncertainty involved in B_i^w , $^{\mathcal{C}_i}P_i$ and $\hat{\mathbf{x}}_i$, we employ the OctoMap, an octotree-based probabilistic framework, to subdivide 3D space into voxels [28]. Each tree node in the octomap has an associated probability indicating how likely the represented voxel is occupied. In our implementation, an individual octomap is created for each crop or weed plant in $\{\mathcal{W}\}$ and is updated for each image frame.
- 2) Candidate Line Segments for Spray Coverage: Droplets sprayed from a narrow-angle nozzle on a moving robot tend to form a line-shaped pattern parallel to the direction of robot motion. It is thus natural to represent a weed occupancy map as a line segment oriented the same as the robot moving direction. For each weed octomap, we first create a discretized version by applying an occupancy probability threshold (Fig. 3(a)) [28]. Voxels with an probability above the threshold is considered occupied. The centers of occupied voxels form a set $O_u = \{o_d : d = 1 \dots D\}$ where $o_d \in \mathbb{R}^3$ is the coordinate of the center of an occupied voxel. We then generate one line segment $l_u = \binom{w}{p_{1,u}}, \stackrel{w}{p_{2,u}}, \stackrel{w}{p_{1,u}} \in \mathbb{R}^3$ and $\stackrel{w}{p_{2,u}} \in \mathbb{R}^3$, from O_u . Define $c_u = \frac{1}{D} \sum_{o_d \in O_u} o_d$ as the centroid. We let l_u go through c_u to make it better represent the location of weed u. $\stackrel{w}{p_{1,u}}$ and $\stackrel{w}{p_{2,u}}$ are calculated as the first and last projected points of O_u onto the direction of robot velocity:

$${}^{\mathcal{W}}\mathbf{p}_{1,u} = \mathbf{c}_u + \min_{\mathbf{o} \in O_u} \left\{ \frac{\langle (\mathbf{o} - \mathbf{c}_u) \cdot {}^{\mathcal{W}} \hat{\mathbf{v}}_i \rangle}{\|{}^{\mathcal{W}} \hat{\mathbf{v}}_i\|} \right\} \frac{{}^{\mathcal{W}} \hat{\mathbf{v}}_i}{\|{}^{\mathcal{W}} \hat{\mathbf{v}}_i\|}, \quad (1)$$

$${}^{\mathcal{W}}\mathbf{p}_{2,u} = \mathbf{c}_u + \max_{\mathbf{o} \in O_u} \left\{ \frac{\langle (\mathbf{o} - \mathbf{c}_u) \cdot {}^{\mathcal{W}} \hat{\mathbf{v}}_i \rangle}{\|{}^{\mathcal{W}} \hat{\mathbf{v}}_i\|} \right\} \frac{{}^{\mathcal{W}} \hat{\mathbf{v}}_i}{\|{}^{\mathcal{W}} \hat{\mathbf{v}}_i\|}, \quad (2)$$

where $\langle A \cdot B \rangle$ is the dot product of vectors A and B. Examples of line segments generated from weed octomaps are illustrated in Fig. 3(b).

The line segments from all currently tracked weeds form a set $L_i = \{l_u : u \in I_i^w\}$ where I_i^w is the index set for weeds contained in the i^{th} image. For each crop, the centroid of the corresponding octomap is estimated the same way. The set of all crop centroids $C_i = \{\mathbf{c}_u : u \in I_i^p\}$ is utilized to determine the importance of each weed where I_i^p is the index set of crops.

3) Feasibility Graph Construction: We further abstract a local DAG G=(V,E) from the current FoV by embracing the feasible nozzle paths among weeds. The vertex set $V=V_n\cup V_w\cup V_d$ is constructed in such a way that the nozzle positions form the graph's starting vertex set V_n , L_i forms the intermediate vertex set V_w , and an additional unit vertex set V_d of the virtual nozzle destination that can be any point in the 3D space (Fig. 4). For the edge set E, an edge $(u,v)\in E$ between two vertices $u,v\in V$ indicates that the nozzle linear acceleration and peak speed allow timely movement from u to v at the current body speed. The virtual destination vertex has edges from all the other vertices, reflecting that not taking actions is an allowed choice for nozzles.

Each position in V_n is either the current nozzle position or the furthest position that has been planned for a nozzle, whichever is further down the robot's moving direction. It is thus updated in

Algorithm 1: K-Nozzle Assignment Algorithm.

Inputs: $L_i = \{l_q = ({}^{\mathcal{W}}\mathbf{p}_{1,q}, {}^{\mathcal{W}}\mathbf{p}_{2,q}) : q = 1 \dots a\};$ $C_i = \{\mathbf{c}_q : q = 1 \dots b\};$ Line segment sequences $\{S_k : k = 1 \dots K\};$ Decision horizon $\mathcal{C}_{i\mathbf{h}} = [0, 0, 1, d]^{\mathsf{T}};$ Graph $G_i = (V_n \cup V_w \cup V_d, E);$ $V_n = \{{}^{\mathcal{W}}\mathbf{p}_k^n : k = 1 \dots K\};$ Outputs: Updated V_n and $\{S_k : k = 1 \dots K\};$

1: for each $u \in V_w$:	O(a)
2: Calculate reward r_u using (4);	O(b)
3: for each $(u,v) \in E$:	$O(a^2)$
4: Calculate cost c_{uv} using (5);	O(1)
5: Formulate BLP using (6a)–(6e);	$O(a^2)$
6: Apply optimization solver [29];	$O(f_{\mathrm{BLP}}(a))$
7: for $k = 1$ to K :	O(K)
8: Traverse the optimal path for nozzle k ;	O(a)
9: if weed l_a in the path reaches c_i h:	

two ways. If the robot has passed the furthest planned position, the algorithm needs to update the position to reflect the current nozzle state. We denote the position of nozzle k as ${}^{\mathcal{W}}\mathbf{p}_k^n \in \mathbb{R}^3$. It is updated as follows,

O(1)

O(1)

$${}^{\mathcal{W}}\tilde{\mathbf{p}}_{k}^{n} = \begin{cases} {}^{\mathcal{W}}\tilde{\mathbf{p}}_{k}^{n} & \text{if } < [0, 1, 0, 0]^{\mathsf{T}} \cdot {}^{\mathcal{W}}_{\mathcal{M}_{i}}\hat{\mathbf{T}}^{-1\mathcal{W}}\tilde{\mathbf{p}}_{k}^{n} > \geq y_{k} \\ {}^{\mathcal{W}}_{\mathcal{M}_{i}}\hat{\mathbf{T}}[x_{k}, y_{k}, z_{k}, 1]^{\mathsf{T}} & \text{otherwise} \end{cases}$$
(3)

where $_{\mathcal{M}_i}^{\mathcal{W}}\hat{\mathbf{T}}\in SE(3)$ is the estimated 4×4 transformation matrix from \mathcal{M}_i to \mathcal{W}, x_k and y_k are the fixed positions of nozzle k along the X-axis and Y-axis of $\{\mathcal{M}\}, z_k$ is the latest position of nozzle k along the Z-axis. Nozzle positions are also updated when new line segments are added to the trajectory sequences of each nozzle, which is detailed in the following section.

B. Optimal K-Nozzle Assignment

 $S_k \leftarrow (S_k, l_q);$ ${}^{\mathcal{W}}\mathbf{p}_k^n \leftarrow {}^{\mathcal{W}}\mathbf{p}_{2,q};$

10:

11:

More emphasis should be placed on weeds that are close to crops, since those weeds compete strongly with crops and are difficult to manage with imprecise approaches. In addition, the extensive motion of nozzles needs to be reduced as it increases wear on the robot mechanism. It should be noted that a globally optimized assignment is infeasible without a global map that contains all the weed locations. Instead, we design a greedy algorithm utilizing the optimal paths of local DAGs to approach the solution obtained with a global DAG. The information available for local solutions is bounded by the observation horizon (i.e. the front of camera FoV) and a decision horizon (i.e. a plane in $\{C_i\}$)(Figs. 3 and 4). Decisions made at the decision horizon ensure that nozzles have time to execute the decisions. If a weed reaching the decision horizon with index u is in the optimal paths, the line segment $l_u \in L_i$ representing the weed will be assigned to the respective nozzle. We wait for more information

before making decisions for weeds not reaching the decision horizon. The decision horizon C_i h is defined as $[0,0,1,d]^T$ where d is the distance of the plane to the origin of $\{C_i\}$. The system performs nozzle assignment at the imaging frequency.

We define the objective function to have two components: the sum of rewards of sprayed weeds and the total distance the nozzles travel on the rails. The reward r_u of $l_u = ({}^{\mathcal{W}}\mathbf{p}_{1,u}, {}^{\mathcal{W}}\mathbf{p}_{2,u}) \in L_i$ is defined as the inverse of the distance from the midpoint of l_u to the closet crop center,

$$r_{u} = \frac{1}{\min_{\mathbf{c}_{q} \in C_{i}} \{ \| \frac{w_{\mathbf{p}_{1,u}} + w_{\mathbf{p}_{2,u}}}{2} - \mathbf{c}_{q} \| \}}.$$
 (4)

The cost c_{uv} of an edge starting from $l_u = ({}^{\mathcal{W}}\mathbf{p}_{1,u}, {}^{\mathcal{W}}\mathbf{p}_{2,u})$ to $l_v = ({}^{\mathcal{W}}\mathbf{p}_{1,v}, {}^{\mathcal{W}}\mathbf{p}_{2,v})$ is defined as the nozzle movement needed along the Z-axis of $\{\mathcal{M}\}$,

$$c_{uv} = |\langle [0, 0, 1]^{\mathsf{T}} \cdot {}^{\mathcal{M}_i}_{\mathcal{W}} \hat{\mathbf{R}}({}^{\mathcal{W}}\mathbf{p}_{2,u} - {}^{\mathcal{W}}\mathbf{p}_{1,v}) \rangle| \tag{5}$$

where $_{\mathcal{W}}^{\mathcal{M}_i}\hat{\mathbf{R}}$ is the estimated 3×3 rotation matrix from $\{\mathcal{W}\}$ to $\{\mathcal{M}_i\}$ and $|\cdot|$ denotes the absolute value.

Denote K as the total number of nozzles on the robot. Let us construct a DAG $G_i = (V_n \cup V_w \cup V_d, E)$ from the current observations and robot state estimation as described in Section V-A3, with $|V_n| = K$. Each edge $(u,v) \in E$ is associated with a cost c_{uv} and each vertex $u \in V_w$ has an associated reward r_u . The objective for the current window is to select K optimal paths with each starting from one of the vertices in V_n and finishing at V_d to maximize the objective function.

We formulate the K-nozzle assignment problem using BLP. Define $\delta^+(u)$ and $\delta^-(u)$ as the sets of outgoing and incoming edges of vertex u, respectively, and decision variables $e_{uv} \in \{0,1\}$ indicate whether the edge from u to v is selected or not in the planned path. The objective of BLP is to optimize over e_{uv} :

$$\underset{e_{uv} \in \{0,1\}}{\text{maximize}} \quad \sum_{v \in V_w} r_v e_{uv} - \sum_{v \in V_w} c_{uv} e_{uv} \tag{6a}$$

subject to $\sum_{(u,v)\in\delta^-(v)}e_{uv}\in\{0,1\}, \forall v\in V_w \tag{6b}$

$$\sum_{(u,v)\in\delta^-(v)}e_{uv}=\sum_{(v,k)\in\delta^+(v)}e_{vk}, \forall v\in V_w \quad (6c)$$

$$\sum_{(u,v)\in\delta^+(u)} e_{uv} = 1, \forall u \in V_n$$
 (6d)

$$\sum_{(u,v)\in\delta^{-}(v)} e_{uv} = K, \forall v \in V_d$$
 (6e)

Constraints in (6b) and (6c) ensure that each weed is visited at most once and the number of incoming paths is equal to that of outgoing paths. The constraint in (6d) enforces that each nozzle must pick a path, while the last constraint in (6e) ensures that each nozzle must arrive at the virtual destination.

The optimization result $\{e_{uv}: (u,v) \in E\}$ defines K paths. Our algorithm then follows each path starting from the nozzle vertices and checks if weeds represented by line segments on the

path have reached the decision horizon. If so, the line segments are assigned to the respective nozzles, and V_n is adjusted to reflect the furthest planned positions. Algorithm 1 shows the pseudocode describing this process.

The BLP is an NP-complete problem, and many algorithms have been developed to solve it. The SCIP framework [29] is employed to solve our problem. If the cardinality of L_i is a, the time complexity to solve the BLP problem can be denoted as $f_{\rm BLP}(a)$. The complexity of our nozzle assignment algorithm is then bounded by $O(f_{\rm BLP}(a))$ as the graph construction, and path traversal can be completed in polynomial time.

C. Trajectory Following

The system performs trajectory following at the IMU's frequency. As soon as the newest $\hat{\mathbf{x}}_j$ and ${}^{W}\hat{\mathbf{v}}_j$ are available, the system checks the first line segment of S_k to determine if the robot has reached the position to spray. If not, the system will let the nozzle move to and stay at a ready position for the upcoming weed. Once the robot is in the proper position, the nozzle will be triggered. If the first line segment has already passed the nozzle, it will be removed from S_k , and the system will repeat the same operation on the next line segment. It is critical to take into consideration the system latency and mitigate its effect. The system latency affecting herbicide spray can be mainly attributed to two aspects: the time it takes to compute $\hat{\mathbf{x}}_i$ from IMU readings and the time it takes for the nozzle valve to respond to the actuation signal. Thus, the system predicts the future position of nozzles based on the past robot state and velocity. The position offset that compensates the system latency can be trivially calculated, so the detailed steps are not elaborated.

VI. EXPERIMENT

Experiments have been conducted both in simulation and field conditions to validate the proposed system. We first show the percentage of weeds that can be sprayed with various numbers of nozzles, body speeds, and weed densities. We then show the spray accuracy using both artificial targets and real plants.

A. Simulation

Monte Carlo simulation has been conducted to determine the percentage of weeds the proposed system can spray in a single pass, given perfect plant detection at different body speeds and weed densities (Fig. 5). Line segments representing weeds with a 5-cm diameter are randomly generated with a uniform distribution on a 20-m long virtual field. Crop plants are uniformly distributed within a 10-cm stripe. The camera FoV is 0.60 × 0.45 m², and the decision horizon is 0.375 m behind the front of the camera FoV. The nozzle peak speed is set at 0.80 m/s. The algorithm proposed in Section V-B is used to assign nozzles to line segments. The robot moves at a constant speed in one direction following the crop row with the camera FoV centered at the crop row. The averaged results of 500 simulation runs are shown in Table I. Here, we report weed coverage within the 10 cm of crop centers as it is the most challenging region for precision weed management [30]. A system with two nozzles

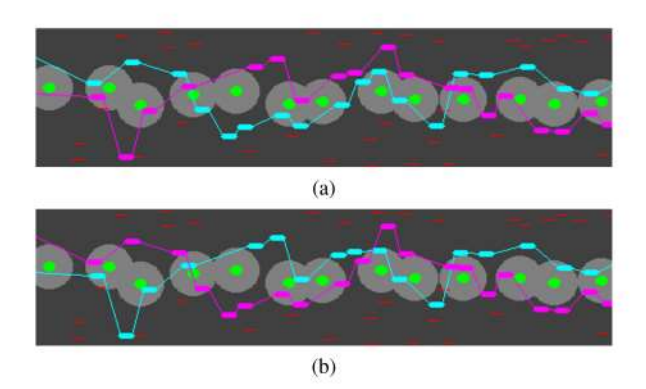


Fig. 5. A section of the virtual field used for simulation. The green dots represent crops with a 5-cm diameter, and the red line segments represent weeds of the same size. The percentage of weeds sprayed by the robot within the gray area (10 cm within the crops) relative to the total weeds within the same area is reported. (a) Results of the K-nozzle assignment algorithm. (b) Solution with a global map.

TABLE I SIMULATION RESULT OF % WEEDS SPRAYED WITHIN 10 CM OF CROP PLANTS AT DIFFERENT ROBOT SPEEDS AND WEED DENSITIES

Nozzle	Speed (m/s)	Weed Density (number/m ²)			
Number		5	10	20	40
1	0.2	96	93	86	75
	0.4	96	91	82	71
	0.6	92	88	79	68
	0.8	91	87	77	63
2	0.2	99	99	99	96
	0.4	99	99	98	93
	0.6	99	99	97	91
	0.8	99	98	96	88
3	0.2	100	100	99	99
	0.4	100	99	99	99
	0.6	100	99	99	98
	0.8	99	99	99	96
4	0.2	100	99	100	99
	0.4	99	100	99	99
	0.6	100	99	99	99
	0.8	99	99	99	99
5	0.2	100	100	99	99
	0.4	100	99	99	99
	0.6	99	99	99	99
	0.8	100	99	99	99

is able to spray more than 95% of weeds in a single pass when the weed density is 20/m². Increasing the nozzle number to 3 on the system can achieve close to 100% coverage of weeds whose distance is less than 10 cm to the crops at a speed of 0.60 m/s.

We perform another Monte Carlo simulation to evaluate the performance of the proposed K-nozzle assignment algorithm in comparison with a naive solution without optimization and the global optimal solution (Fig. 6). The global optimal solution is obtained using the same K-nozzle assignment algorithm assuming the global map is available, while the naive algorithm assigns the nozzles to the nearest reachable weeds when weeds reach the decision horizon. The total reward of sprayed weeds minus the total lateral movement of nozzles for the whole virtual field is used to compare the optimality and is calculated similarly to (6a). The simulation settings are the same as in the previous simulation experiment. A total of 500 iterations were conducted. The comparison results show that the proposed

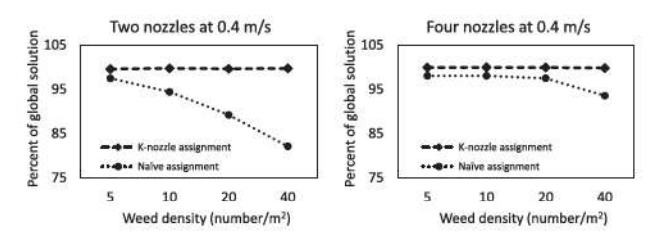


Fig. 6. Results of Monte Carlo simulation to compare the total rewards of sprayed weeds minus the total lateral movement of nozzles among three approaches: assignment based on a global map, K-nozzle assignment, and assignment by a naive algorithm. The percentage is relative to the values of the global assignment.

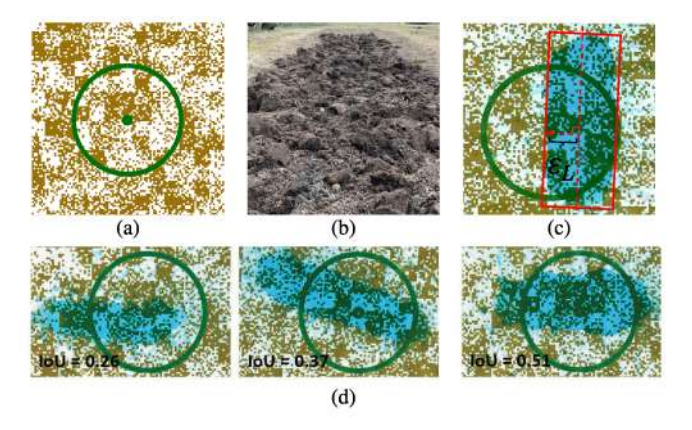


Fig. 7. (a) The paper target used for accuracy evaluation. (b) The field condition used in the accuracy experiment. (c) A sprayed paper target and the error metrics used for evaluation. (d) Examples of sprayed paper targets with IoU of 0.26, 0.37, and 0.51 from left to right.

K-nozzle assignment algorithm can closely approach the global solution while the performance of the naive algorithm decreases as the weed density increases. Other combinations of nozzle number and robot speed show a similar pattern, so the results are not explicitly presented.

B. Spray Accuracy Physical Experiments

To test the accuracy of the proposed system, we design a paper target, which has a circle with a dot at the center representing the weed (Fig. 7(a)). The circle has a diameter of 5 cm, a typical size of weeds in an early growth stage. Paper targets are placed in the real field to recreate real field surface conditions (Fig. 7(b)). During each trial, ten paper targets were placed randomly on a 0.6×10 m² path, and the robot was manually controlled to follow the path. The time for the system to travel from the start point of the path to the end was recorded, and the average speed was reported. A total of 10 trials were conducted, with average speeds ranging from 0.28 m/s to 0.73 m/s. Blue dye was added to the liquid to better visualize the region sprayed. After each trial, the paper targets were scanned for evaluation.

Examples of the sprayed paper targets are shown in Fig. 7(d). Two metrics are used: lateral offset ε_L and Intersection over Union (IoU). ε_L measures how accurately the system can perceive the location of weeds to guide herbicide spray, while IoU measures how well the system can cover each weed without

TABLE II EVALUATION OF SPRAY ACCURACY AT VARIOUS SPEEDS

Trial ID	Speed (m/s)	ε_L (cm)		IoU	
		Mean	Std.	Mean	Std.
1	0.28	0.62	0.30	0.40	0.05
2	0.32	0.74	0.13	0.40	0.04
3	0.36	0.73	0.24	0.35	0.04
4	0.37	0.43	0.23	0.42	0.06
5	0.44	0.25	0.11	0.45	0.05
6	0.46	0.68	0.33	0.40	0.07
7	0.50	0.46	0.35	0.35	0.05
8	0.55	0.40	0.23	0.33	0.02
9	0.66	0.56	0.30	0.26	0.06
10	0.73	0.45	0.37	0.25	0.01



Fig. 8. Photos of a section of the test field with real plants. Top row: overview of the section with pea plants growing in a row and mustard plants (weeds) around them; second and third rows: close-up photos of the sprayed mustard plants with blue dye indicating the sprayed area.

wasting herbicides. The minimum-area bounding rectangles of the sprayed regions are calculated, and their axes are used to estimate the trajectories the nozzles have followed. ε_L is then calculated as the distance from the center of the circle pattern to the rectangle axis (Fig. 7(c)). IoU is calculated between the circle pattern and the sprayed pattern. The average ε_L and IoU of each trial and their standard deviation are reported in Table II. Average ε_L at all speeds remained below 1 cm, which is sufficiently accurate considering the uneven soil surface. However, the IoU tends to decrease as the speed goes beyond 0.5 m/s, mainly due to the reduced amount of liquid delivered onto a unit area and the increased error of the starting and ending positions for each spray pulse.

Since it is difficult to quantitatively measure the spray accuracy on real plants, we instead qualitatively demonstrate the system in field conditions. Winter pea (*Pisum sativum*) was planted as the crop, and mustard (*Brassica juncea*) was planted as the weed in the same field as that of the spray accuracy experiment. The average diameter was around 7 cm for the pea plants and 4 cm for the mustard plants. Weed density is roughly $10/m^2$ and the crop spacing is 20 cm. The plant size, weed distribution, and soil surface condition are similar to a common crop production field with early-stage crops and low-density weeds. The proposed system traveled at 0.4 m/s during testing. The quality of herbicide spray is shown in Fig. 8. It can be seen

from the close-up photos that the lateral accuracy and the leaf coverage by the herbicide droplets are satisfactory in challenging field conditions.

C. Comparison Study

The herbicide spray system most similar to ours in the literature is the system designed by Wu et al. [6]. For the field experiment, Wu et al. only tested their system up to 0.4 m/s, as shown in Table 5 of their paper. Our algorithm and hardware designs allow the proposed system to travel almost twice as fast (0.73 m/s as shown in Table II) while maintaining a high accuracy and droplet coverage on weeds. For spray accuracy, since there is no quantitative experiment conducted by Wu et al., direct comparison between their system and ours is difficult. We instead qualitatively compare our spray accuracy in Fig. 8 to theirs. It is not difficult to notice that our system has better positional accuracy and finer resolution. Therefore, our system achieves higher efficiency and accuracy for robotic herbicide application.

VII. CONCLUSION AND FUTURE WORK

We developed a robotic system that sprays micro-volume herbicide for weed control on a mobile robot. To facilitate decision-making, the crop/weed scene is represented by candidate spray line segments. We further abstract a DAG embracing the information of feasible paths among weeds from the scene. We propose a K-nozzle assignment/motion planning problem in algorithm development. We present an algorithm based on BLP that maximizes spray coverage within the adjacent areas of crops. Tests on artificial targets in field conditions at various speeds showed sub-centimeter lateral error. Field evaluation on real plants demonstrated high spray quality. In the future, we will investigate multi-actuator assignments and even multi-robot coordination to improve system performance. We will develop better scene representation methods for different types of weeds. We will combine robot motion planning and nozzle planning problems together to fully optimize the system performance.

REFERENCES

- E.-C. Oerke, "Crop losses to pests," J. Agric. Sci., vol. 144, no. 1, pp. 31–43, 2006.
- [2] S. A. Fennimore, D. C. Slaughter, M. C. Siemens, R. G. Leon, and M. N. Saber, "Technology for automation of weed control in specialty crops," Weed Technol., vol. 30, no. 4, pp. 823–837, 2016.
- [3] D. C. Slaughter, D. Giles, and D. Downey, "Autonomous robotic weed control systems: A review," *Comput. Electron. Agr.*, vol. 61, no. 1, pp. 63–78, 2008.
- [4] M. V. Bagavathiannan, J. K. Norsworthy, K. L. Smith, and P. Neve, "Modeling the evolution of glyphosate resistance in barnyardgrass (echinochloa crus-galli) in cotton-based production systems of the midsouthern United States," Weed Technol., vol. 27, no. 3, pp. 475–487, 2013.
- [5] S. Xie, C. Hu, M. Bagavathiannan, and D. Song, "Toward robotic weed control: Detection of nutsedge weed in bermudagrass turf using inaccurate and insufficient training data," *IEEE Robot. Autom. Lett.*, vol. 6, no. 4, pp. 7365–7372, Oct. 2021.
- [6] X. Wu, S. Aravecchia, P. Lottes, C. Stachniss, and C. Pradalier, "Robotic weed control using automated weed and crop classification," J. Field Robot., vol. 37, no. 2, pp. 322–340, 2020.

- [7] G. V. Nardari et al., "Place recognition in forests with urquhart tessellations," *IEEE Robot. Autom. Lett.*, vol. 6, no. 2, pp. 279–286, Apr. 2021.
- [8] E. Marks, F. Magistri, and C. Stachniss, "Precise 3D reconstruction of plants from UAV imagery combining bundle adjustment and template matching," in *Proc. IEEE Int. Conf. Robot. Autom.*, Philadelphia, PA, USA, May 2022, pp. 2259–2265.
- [9] A. N. Sivakumar et al., "Learned visual navigation for under-canopy agricultural robots," in Proc. Robot.: Sci. Syst., 2021.
- [10] P. Maini, B. M. Gonultas, and V. Isler, "Online coverage planning for an autonomous weed mowing robot with curvature constraints," *IEEE Robot. Autom. Lett.*, vol. 7, no. 2, pp. 5445–5452, Apr. 2022.
- [11] X. Liu et al., "Large-scale autonomous flight with real-time semantic SLAM under dense forest canopy," *IEEE Robot. Autom. Lett.*, vol. 7, no. 2, pp. 5512–5519, Apr. 2022.
- [12] T. C. Thayer, S. Vougioukas, K. Goldberg, and S. Carpin, "Multirobot routing algorithms for robots operating in vineyards," *IEEE Trans. Autom.* Sci. Eng., vol. 17, no. 3, pp. 1184–1194, Jul. 2020.
- [13] W. McAllister, J. Whitman, J. Varghese, A. Davis, and G. Chowdhary, "Agbots 3.0: Adaptive weed growth prediction for mechanical weeding agbots," *IEEE Trans. Robot.*, vol. 38, no. 1, pp. 556–568, Feb. 2022.
- [14] W. S. Lee, D. Slaughter, and D. Giles, "Robotic weed control system for tomatoes," *Precis. Agric.*, vol. 1, no. 1, pp. 95–113, 1999.
- [15] T. Utstumo et al., "Robotic in-row weed control in vegetables," Comput. Electron. Agr., vol. 154, pp. 36–45, 2018.
- [16] R. Raja, D. C. Slaughter, S. Fennimore, and M. Siemens, "Precision weed control robot for vegetable fields with high crop and weed densities," in *Proc. ASABE Annu. Int. Meet. Amer. Soc. Agricultural Biol. Engineers*, 2019, Art. no. 1.
- [17] G. Jocher et al., "ultralytics/yolov5: V6.0," Oct. 2021. [Online]. Available: https://doi.org/10.5281/zenodo.5563715
- [18] J. Yuan, J. Hong, J. Sattar, and V. Isler, "ROW-SLAM: Under-canopy cornfield semantic SLAM," in *Proc. Int. Conf. Robot. Autom.*, May 2022, pp. 2244–2250.
- [19] D. C. Conner, A. Greenfield, P. N. Atkar, A. A. Rizzi, and H. Choset, "Paint deposition modeling for trajectory planning on automotive surfaces," *IEEE Trans. Autom. Sci. Eng.*, vol. 2, no. 4, pp. 381–392, Oct. 2005.
- [20] D. Gleeson et al., "Generating optimized trajectories for robotic spray painting," *IEEE Trans. Autom. Sci. Eng.*, vol. 19, no. 3, pp. 1380–1391, Jul. 2022.
- [21] D. Song, A. van der Stappen, and K. Goldberg, "Exact algorithms for single frame selection on multiaxis satellites," *IEEE Trans. Autom. Sci. Eng.*, vol. 3, no. 1, pp. 16–28, Jan. 2006.
- [22] H. Wang and B. Alidaee, "Unrelated parallel machine selection and job scheduling with the objective of minimizing total workload and machine fixed costs," *IEEE Trans. Autom. Sci. Eng.*, vol. 15, no. 4, pp. 1955–1963, Oct. 2018.
- [23] P. Chalasani, R. Motwani, and A. Rao, "Algorithms for robot grasp and delivery," in *Proc. 2nd Int. Workshop Algorithm. Found. Robot.*, 1996, pp. 347–362.
- [24] K. Gao and J. Yu, "Capacitated vehicle routing with target geometric constraints," in *Proc. IEEE/RSJ Int. Conf. Intell. Robot. Syst.*, 2021, pp. 7925–7930.
- [25] A. Bewley, Z. Ge, L. Ott, F. Ramos, and B. Upcroft, "Simple online and realtime tracking," in *Proc. IEEE Int. Conf. Image Process.*, 2016, pp. 3464–3468.
- [26] H. Hirschmuller, "Stereo processing by semiglobal matching and mutual information," *IEEE Trans. Pattern. Anal. Mach. Intell.*, vol. 30, no. 2, pp. 328–341, Feb. 2008.
- [27] T. Qin, J. Pan, S. Cao, and S. Shen, "A general optimization-based framework for local odometry estimation with multiple sensors," 2019, arXiv:1901.03638.
- [28] A. Hornung, K. M. Wurm, M. Bennewitz, C. Stachniss, and W. Burgard, "OctoMap: An efficient probabilistic 3D mapping framework based on octrees," *Auton. Robot.*, vol. 34, no. 3, pp. 189–206, 2013.
- [29] T. Achterberg, "SCIP: Solving constraint integer programs," Math. Program. Comput., vol. 1, no. 1, pp. 1–41, 2009.
- [30] M. Perez-Ruiz, D. C. Slaughter, F. A. Fathallah, C. J. Gliever, and B. J. Miller, "Co-robotic intra-row weed control system," *Biosyst. Eng.*, vol. 126, pp. 45–55, 2014.